Rectangular pulse generation based on pulse reshaping using a superstructured fiber Bragg grating

P. Petropoulos, M. Ibsen, A.D. Ellis[1], and D.J. Richardson

Optoelectronics Research Centre, University of Southampton, Southampton SO17 1BJ, U.K.

[1] Corning Research Centre, Adastral Park, Martlesham Heath, Ipswich IP5 3RE, U.K.

Tel.: +44 2380 593141

Fax: +44 2380 593142

E-mail: pp@orc.soton.ac.uk

Abstract

In this paper we present a technique for the shaping of short pulses based on the use of superstructured fibre Bragg gratings. We apply this technique to demonstrate the generation of 20ps rectangular pulses by phase and amplitude profiling of 2.5ps soliton pulses. Numerical calculations validate our experimental findings.

Keywords: Fiber gratings, optical pulse shaping, optical signal processing, optical fiber filters, optical fiber communication

1

Rectangular pulse generation based on pulse reshaping using a superstructured fiber Bragg grating

P. Petropoulos, M. Ibsen, A.D. Ellis[1], and D.J. Richardson

Optoelectronics Research Centre, University of Southampton, Southampton SO17 1BJ, U.K.

[1] Corning Research Centre, Adastral Park, Martlesham Heath, Ipswich IP5 3RE, U.K.

E-mail: pp@orc.soton.ac.uk

Introduction

Recent advances in the area of ultrafast optics, and in particular the area of optical communications, demand new techniques for the precise control and manipulation of the shape of optical pulses. For example the generation of well-defined pulse forms and pulse sequences are required for a wide range of spectroscopic pump probe experiments, such as the coherent excitation and control of optically-induced quantum states within semiconductor materials and devices. In the telecommunications arena a typical example occurs within dispersion managed soliton systems where it is desirable to pre-shape (pre-chirp) the optical pulse at the input to the transmission line so as to minimize the generation of dispersive radiation along the system and to achieve optimum system performance.

In order to 'synthesize' a particular optical pulse form one needs to be able to reliably define the amplitude and phase profile of an optical field. The general approach is to generate pulses with a well-defined pulse form and to then pass the pulse through some pulse shaping element with an appropriately designed transfer function to re-phase and re-shape the incident spectrum so as to obtain the desired output optical field. The pulse-shaping element can have a pure linear response such as a filter with a suitably complex reflectivity response, or might additionally include a nonlinear element, e.g. an optical fiber [1] or an aperiodic quasi-phase matched structure [2], to allow the controlled generation of frequency components outside the frequency spectrum of the input pulse-form.

The most commonly used technique is a simple linear filtering technique in which the frequency components of a short pulse are spatially dispersed using bulk gratings, and then filtered by means of amplitude and phase-masks positioned within a Fourier optical 4f set-up [3]. Microlithographically fabricated spatial-masks [4], segmented liquid crystal modulators [5], or acousto-optic modulators [6] have been used as spatial filters, the latter two approaches allowing for programmability and dynamic reconfigurability of the pulse shaping response. Whilst impressive results are possible with this approach the hardware itself is somewhat bulky, lossy and expensive and does not lend itself to ready integration with waveguide devices. These issues have prompted the search for other technical approaches to the problem such as the use of arrayed waveguide gratings [7], and arrays of fiber delay lines [8].

SuperStructured Fiber Bragg Gratings (SSFBGs) can also be considered and employed as spectral filters of controllable phase and amplitude. The term SSFBG generally refers to a fiber Bragg grating whose refractive index profile is not uniform in amplitude and/or phase along its length. For ease of discussion, we restrict the following discussion to the weak grating limit in which the relative changes of its refractive index are small enough to allow the incident light to penetrate the full device length such that the whole grating contributes equally to the reflected signal. However, it should be appreciated that due to recent advances in grating design algorithms the general principles outlined below can now be readily applied to the high reflectivity, non-Fourier design limit [9] - the required grating designs are just less physically obvious. For a weak SSFBG the wavevector response $F(\kappa)$ is given by the Fourier transform of the spatial refractive index modulation profile $A(x)$ used to write the grating [10, 11], where κ is the wavevector, which is proportional to the frequency ω, i.e.

$$F(\kappa) = \frac{1}{2\pi} \int_{-\infty}^{+\infty} A(x)e^{j\kappa x} dx .$$

(Eq.1)

The impulse response $h(t)$ of a fiber grating is given by the inverse Fourier transform of its frequency response $H(\omega)$

$$h(t) = \int_{-\infty}^{+\infty} H(\omega)e^{-j\omega t} d\omega .$$

(Eq.2)

It follows that the impulse response $h(t)$ of a weak FBG is a pulse of the same temporal profile as the spatial modulation profile $A(x)$ of the grating (with an appropriate conversion from the space to time frame via $t = 2x\,n/c$, where n is the refractive index of the fiber core). The (reflected) optical response $y(t)$ of the grating to a pulse of finite time duration $x(t)$ is given simply by the convolution of the input signal with the grating's impulse response i.e.

$$y(t) = x(t) * h(t) . \qquad\qquad \text{(Eq.3)}$$

Alternatively, as expressed in the frequency domain, the reflected signal $Y(\omega)$ is the product of the incident signal $X(\omega)$ with $H(\omega)$

$$Y(\omega) = X(\omega)H(\omega) \qquad\qquad \text{(Eq.4)}$$

where $Y(\omega)$ and $X(\omega)$ imply the Fourier transforms of $y(t)$ and $x(t)$ respectively. Thus it can be appreciated that, for well-specified input and target output pulse forms, one can (subject to the usual laws of causality and the limits of FBG technology) design and fabricate an FBG to perform the required shaping operation. SSFBGs are attractive for many pulse shaping applications since they offer all the advantages associated with fiber components, such as ready integration into fiber systems and low coupling losses. Moreover, they are potentially low-cost devices.

This concept has been used in the past, in conjunction with conventional uniform FBG designs, to generate a train of dark pulses [12], and to obtain a matched filter for the detection of 100ps square pulses [13]. However, advances in the fabrication of FBGs now allow the fabrication of gratings with truly complicated amplitude and phase characteristics, greatly extending the potential and range of applications of the approach. For example, we recently demonstrated pattern generation and recognition [14], as required for optical code division multiple access applications (OCDMA), and have also demonstrated the use of an FBG to perform pulse repetition rate multiplication from 10 to 40 GHz [15], using what should still be considered relatively simple SSFBG structures.

In this work, we demonstrate the fabrication and use of a truly complex superstructure grating designed to transform short optical pulses (2.5ps at 10GHz) into a corresponding train of 20ps rectangular pulses. Such pulse forms are required for nonlinear optical switching applications, in which a square switching window is desired. The results achieved highlight the quality of the "continuous grating writing" technique and establish the superstructure technique as a viable means for achieving a broader range of pulse shaping functions than had generally been considered technologically feasible.

Filter design

Since our pulse shaping technique is a purely passive-filtering process we require a well-defined input pulse form to filter and thereby reliably re-shape. For our experiments we

6

chose to use pulses generated by an actively mode-locked erbium doped fiber ring laser containing anomalously dispersive fiber and which naturally generates high-quality optical solitons by virtue of its principle of operation. Our target output waveform was square pulses with 20ps duration. We chose this particular pulse duration to ensure that we could accommodate an adequate number of spectral features within the finite available spectral bandwidth defined by the input pulse form and SSFBG reflectivity bandwidth. (The input pulse duration in our experiments was 2.5ps (full width at half maximum - FWHM) and we restricted the SSFBG bandwidth to 6nm, which represents the -40dB spectral bandwidth for such pulses).

In Figs.1a and b we plot the spectrum and pulse shape of the electric field distribution associated with our choice of input and output pulse forms which should clarify the discussion. The spectrum of an idealized square pulse is a sinc function, which exhibits lobed features of alternating optical phase. For our particular choice of relative pulse durations we can accommodate 13 spectral lobes within the available 6nm spectral bandwidth. By retaining a significant number of features (and associated broadband spectral components) we can obtain fast rise and fall times on the pulses as seen in Fig.1b. The spectral truncation gives rise to the development of 'ringing structure' close to the square pulse edges in the time domain (Gibbs phenomenon). In designing our grating we have sought to minimize these effects by gently apodizing the output spectrum using a Gaussian profile [16], so that the targeted signal follows the mathematical specification:

$$Y(\omega) = \frac{\sin(p\omega)}{p\omega} \cdot e^{-(a\omega)^2} . \qquad\qquad\text{(Eq.5)}$$

The factor p in this equation determines the spectral width, and in our case was set to 9.87THz^{-1}. The expense of introducing apodization is a slight increase in the rise and fall times of the pulses. The apodization factor a was hence kept fairly small, namely 0.55THz^{-1}, to give a satisfactory trade-off between the two undesirable effects. The 10 – 90% rise/fall times of our target pulses were 1.6ps and the relative ripple depth was 0.03 (Fig.1b). The corresponding figures for non-apodized pulses are rise/fall times of 1.0ps and a relative ripple depth of 0.24. Note here that we define the relative ripple depth as the ratio of the difference between the highest and lowest intensity points of the ripple at the top of the square pulses to the maximum intensity of the pulses.

The required response of the FBG in the frequency domain $H(\omega)$ could then be easily calculated from Eqn.4 as the quotient of the output $Y(\omega)$ (desired) to the input frequency spectrum of ideal soliton pulses $X(\omega)$. A plot of the desired reflectivity response is shown in Fig.2b (dashed line). The corresponding refractive index superstructure required to achieve this response is obtained from inverting Eqn.1 and is shown in Fig.2a, and highlights the precision required of the grating writing process. Note that the sections of negative induced index are achieved experimentally by putting additional discrete phase shifts into the structure such that a positive index change from the base line level can be used over the entire grating length [16]. The length of the grating in the time domain was $t = 100\text{ps}$, corresponding to a grating length of $0.5\,t\,c/n = 10.3\text{mm}$.

We tested numerically the sensitivity of the shaping operation to a variety of non-ideal optical excitation conditions, and grating fabrication defects (by non-ideal we mean differing in some regard from the design input pulse form).

Firstly, we investigated the effect of using pulses with a soliton pulse shape, but a duration differing from the duration used for the SSFBG design. The analysis showed that small (+/- 20%) departures of the pulse width from the ideal 2.5ps affected the trade-off between ripple strength and rise/fall time (see Fig.3a). Specifically, the ringing structure on the filtered pulses becomes more dominant for shorter pulses, whereas for wider pulses the rising and falling edges of the output pulses become less sharp and they begin to lose their flat-top nature. This behavior is easily understood by visualizing the signals in the frequency domain: The result of using shorter pulses, which exhibit a wider bandwidth, is to partially cancel out the apodization. Similarly, using broader pulses, which exhibit a narrower bandwidth, imposes additional apodization on the output pulses.

Secondly, we investigated the use of pulses with the desired half width but with pulse shapes that differ significantly from the desired transform limited soliton form. The pulses used to generate Fig.3b correspond to 2.5ps linearly chirped soliton pulses with a different chirp parameter C as defined below:

$$x(t) = \sec h(\frac{1.763t}{\Delta T}) \cdot e^{-\frac{j1.554Ct^2}{\Delta T^2}} \qquad \text{(Eq.6)}$$

where ΔT is the FWHM of the pulses [17]. The performance of the filter is seen to be reasonably good for relatively small amounts of chirp ($C \leq 0.1$), however for more extreme chirps the pulse deformation becomes more severe and spikes begin to develop at the leading and trailing edges. The performance of the filter was also examined with transform-limited Gaussian input pulses of various widths (Fig.3c). Gaussian pulses are characterized by a wider spectrum than those of soliton pulses of the same FWHM. For 2.5ps Gaussian input pulses the deformation of the filtered output is quite significant and is characterized by the formation of sharp spikes on the pulse edges. By contrast we find that if we use Gaussian pulses with the same 3dB spectral width as a 2.5ps soliton (the pulse duration in this instance is 3.55ps), then the response closely resembles the idealized case. There is however a slight compromise in the rise and fall times, and the pulses exhibit slight spikes close to the edges (see Fig.3c).

We also examined the case of a mismatch between the central wavelength of the SSFBG to that of the incoming pulses (see Fig.3d). Significant distortion of the pulses only becomes evident for wavelength mismatches greater than ~0.3nm, and again manifests itself as the formation of dominant spikes at the pulse edges. Moreover, the intensity of the central part of the pulse is decreased. For more extreme mismatch cases (e.g. 1.5nm) the spike formation is so severe that the reflected waveform effectively divides into two distinct pulses.

Finally, we examined numerically the effect that potential imperfections in the SSFBG structure could have on the shaping action. Grating imperfections can arise either due to

errors associated with the UV exposure itself (e.g. laser power fluctuations, phase mask errors), or from small variations in the fiber core diameter [18]. For our particular writing technique the latter source of error is deemed the most likely. Such imperfections manifest themselves as both phase and amplitude errors in the complex SSFBG superstructure function. It is difficult to estimate reliably the contribution of these imperfections. However, in order to gain an insight we simulated their effect by adding noise (both phase and amplitude) to the SSFBG refractive index profile. For the purpose of our calculations we assumed the phase and amplitude noise to be independent of each other, and to be randomly distributed along the grating length subject to a normal distribution with well defined mean and variance. Mathematically then we modified the local values of the ideal grating superstructure function by:

$$A_n(x) = \mid A_0(x) \mid \cdot n_1(x) \cdot e^{-j(\arg(A_0(x)) + 2\pi n_2(x))} \qquad \text{(Eq.7)}$$

where $A_0(x)$ is the ideal superstructure function, and $n_1(x)$ and $n_2(x)$ are the random amplitude and phase noise parameters respectively. The temporal shapes of two extreme cases of distorted pulses generated from the 'noisy' structures are shown in Fig.4. The value of the phase noise parameter $n_2(x)$ used to generate fig.4, had a mean value of 0 and a standard deviation of 0.04, whereas the amplitude noise $n_1(x)$ was ascribed a mean value of 1 and a standard deviation of 0.02. Note that these figures should be considered as extremely large for such a short FBG and the "continuous grating writing" technique employed. However, even with such a large noise contribution it can be seen that its

effects are still somewhat minimal, further confirming the robustness of the shaping action.

Examining the various individual plots presented in Fig.3 and Fig.4 it is clear that our shaping mechanism is reasonably robust and not particularly sensitive to the precise pulse excitation parameters, or small deviations in grating design. Indeed all of the estimated tolerances are well within readily achievable experimental limits, as we demonstrate below.

Experiments

Our experimental set up is shown in Fig.5. An all-polarization-maintaining harmonically mode-locked erbium fiber ring laser operating at a repetition rate of 10GHz [19] was used to generate the input pulses. The central wavelength of the laser was tunable through the use of an intra-cavity band-pass filter. In Fig.6 we show inset the optical spectrum of the pulses which have a 3dB bandwidth of 1.0nm. The input spectrum is composed of discrete, infinitely narrow spectral lines separated by ~0.8nm corresponding to the signal repetition rate – these lines are clearly resolved in this high-resolution scan (resolution: ~25pm). The corresponding autocorrelation trace of the input pulses is shown in Fig.7a where it is seen that they have a FWHM of 2.5ps. This yields an estimated time-bandwidth product (TBP) of ~0.32 giving us confidence that the pulses are indeed close to transform-limited solitons. The pulses were launched through a short length of fiber

onto the SSFBG via a 3-port optical circulator. The resulting pulse shaping effects upon reflection from the SSFBG were investigated in the time and frequency domains at the circulator output port. The SSFBG was mounted on a rig to allow for fine strain-tuning of its central wavelength relative to that of the source. The SSFBG was fabricated using the "continuous grating writing" technique that allows the continuous writing of long and complex profiled gratings on a plane by plane basis [20]. The reflectivity of the grating was kept relatively low (~10%) to ensure that we operated well within the Fourier limit. A plot of the amplitude and time delay response of the resulting structure is shown in Figs.2b and 2c respectively, as measured with an optical network analyzer. The target theoretical reflectivity spectrum is also shown superposed on Fig.2b - the agreement with the experimentally measured curve is seen to be excellent. Direct evidence for the discrete phase jumps between the individual reflectivity lobes of the grating is given by the observation of sharp features in the time delay response at the lobe edges as seen in Fig.2c. The flatness of the time delay response within the lobe pass band, albeit limited by system measurement noise/resolution, also provides a good indication of a uniform phase response across the main body of the individual lobes as desired.

The power spectrum of the pulses reflected from the FBG is shown in Fig.6a. This is compared to the spectrum of the single square pulse expected from the design procedure (Fig.6b). There is a very good agreement between the envelopes of the two spectra even at levels ~25dB below the main spectral peak. (The distinct spectral lines of the experimental trace arise from the high repetition rate of the signal, which was not taken into account on the calculated filter response and are readily resolved by the spectrum

13

analyzer). The temporal shape of the reflected pulses was initially evaluated using an autocorrelator. The intensity autocorrelation function of a square pulse of duration T is a triangular pulse of total duration 2T. An autocorrelation trace of the filtered pulses is shown in Fig.7b, and is compared to the calculated autocorrelation function of the targeted waveform (Fig.7c), and an autocorrelation trace of the input pulses (Fig.7a). The shaping action of the FBG can easily be appreciated. The full width of the triangular ACF is ~40ps as expected for a 20ps pulse form.

To establish the quality of the shaping more directly we conducted measurements using an optical sampling oscilloscope. The system used an electroabsorption modulator and an electronically driven delay circuit to sample the optical signal at delayed times relative to the fixed RF drive to the laser [21]. The resolution of this device was ~7ps as determined by measurements of the incident 2.5ps pulse forms (Fig.8a). The measurement on the pulses reflected from the SSFBG is shown in Fig.8b where it is seen that reasonably square 20ps pulse forms are obtained. An accurate estimate of the rise and fall times on the pulse is limited by the 7ps temporal resolution of the measurement apparatus. There appears to be slight amplitude variation (~5-10%) across the top of the pulses. At this stage it is not yet established whether this variation is due to grating imperfections, or is an artifact of the optical sampling scope set up. Nevertheless, the main targets of the shaping operation, i.e. the generation of an almost flat top and sharp edges, are clearly demonstrated.

14

In additional experiments we detuned the central wavelength of the source relative to that of the SSFBG, and diagnosed the filtered signal using the optical sampling oscilloscope and an optical spectrum analyzer. The results of these measurements are summarized in Fig.9. These should be compared to the numerical calculations presented in Fig.3d, (taking into account of course the limited resolution of the optical oscilloscope). The two cases shown in Fig.9 are for an incoming signal of central wavelength 0.4 and 1.4nm away from the central wavelength of the SSFBG respectively. The general behavior predicted in Fig.3d is confirmed here, with the central part of the pulse decreasing, until the pulse splits into two parts.

Finally, we performed Bit-Error-Rate (BER) measurements at 10Gbit/s using the square pulses. For these measurements, the 10GHz laser signal was modulated using a 2^{31}-1 pseudorandom bit sequence before being coupled onto the SSFBG. The reflected signal was detected using a commercial 10Gbit/s RZ photoreceiver and fed to the BER tester. The BER measurements are summarized in Fig.10, where it is shown that error free operation was readily achieved down to the 10^{-11} level, with only a slight (< 0.5dB) power penalty relative to back to back measurements on the laser source.

Conclusion

In conclusion, we have demonstrated high-quality, soliton to square pulse conversion using reflection from a complex superstructure grating with an appropriately designed amplitude and phase response and found the performance to be in good agreement with

15

our predictions. In addition, we investigated theoretically the tolerance of the proposed scheme to various non-ideal excitation conditions, and to random grating writing errors and showed it to be reasonably robust on both counts. We consider the main significance of the results to be that they highlight the capability of advanced grating writing technology for use in pulse shaping applications within the communications arena. Square pulse generation is itself of intrinsic interest for a range of nonlinear all-optical switching and frequency conversion applications.

References

[1]   N.J. Halas, D. Krökel, and D. Grischkowsky, "Ultrafast light-controlled optical-fiber modulator", Appl. Phys. Lett., vol. 50, pp. 886-888, 1987.

[2]   G. Imeshev, A. Galvanauskas, D. Harter, M.A. Arbore, M. Proctor, and M.M. Fejer, "Engineerable femtosecond pulse shaping by second-harmonic generation with Fourier synthetic quasi-phase-matching gratings", Opt. Lett., vol.23, pp. 864-866. 1998.

[3]   A.M. Weiner, and A.M. Kan'an, "Femtosecond pulse shaping for synthesis, processing, and time-to-space conversion of ulatrafast optical waveforms", IEEE J. Sel. Topics in Quantum Electron., vol. 4, pp. 317-331, 1998.

[4]   A.M. Weiner, J.P. Heritage, and E.M. Kirschner, "High-resolution femtosecond pulse shaping", J. Opt. Soc. Am. B, vol. 5, pp. 1563-1572, 1988.

[5]   A.M. Weiner, D.E. Leaird, J.S. Patel, and J.R. Wullert, "Programmable shaping of femtosecond pulses by use of a 128-element liquid-crystal phase modulator", IEEE J. Quantum Electron., vol. 28, pp. 908-920, 1992.

[6]   M.R. Fetterman, D. Goswami, D. Keusters, W. Yang, J.-K. Rhee, and W.S. Warren, "Ultrafast pulse shaping: amplification and characterization", Opt. Express, vol. 3, pp. 366-375, 1998.

[7]   H. Tsuda, H. Takenouchi, T. Ishii, K. Okamoto, T. Goh, K. Sato, A. Hirano, T. Kurokawa, and C. Amano, "Spectral encoding and decoding of 10Gbit/s femtosecond pulses using high resolution arrayed-waveguide grating", Electron. Lett., vol. 35, pp. 1186-1188, 1999.

[8]   G.J. Pendock, M.J.L. Cahill, and D.D. Sampson, "Multi-gigabit per second demonstration of photonic code-division multiplexing", Electronics Lett., vol. 31, pp. 819-820, 1995.

[9]   R. Feced, M.N. Zervas, and M.A. Muriel, "An efficient inverse scattering algorithm for the design of nonuniform fiber Bragg gratings", IEEE J. Quantum Electron., vol.35, pp.1105-1111, 1999.

[10]   K.O. Hill, and G. Meltz, "Fiber Bragg grating technology fundamentals and overview", J. Lightwave Technol., vol. 15, pp. 1263-1276, 1997.

[11]   B.J. Eggleton, P.A. Krug, L. Poladian, and F. Ouellette, "Long periodic superstructure Bragg gratings in optical fibres", Electron. Lett., vol. 30, pp.1620-1622, 1994.

[12]   Ph. Emplit, M. Haelterman, R. Kashyap, and M. De Lathouwer, "Fiber Bragg grating for optical dark soliton generation", IEEE Photon. Technol. Lett., vol. 9, pp. 1122-1124, 1997.

[13]   H. Geiger, M. Ibsen, and R.I. Laming, "Optimum receivers with fibre gratings", Technical Digest OFC'98, San Jose, paper WI2, p. 152.

[14]   P.C. Teh, P. Petropoulos, M. Ibsen, and D.J. Richardson, "A 10Gbit/s, 160Gchip/s OCDMA system based on superstructured fiber gratings", Technical Digest OFC'2000, Baltimore, postdeadline paper PD9.

[15]   P. Petropoulos, M. Ibsen, D.J. Richardson, and M.N. Zervas, "Generation of a 40 GHz pulse stream by pulse multiplication using a sampled fiber Bragg grating", Opt. Lett., vol. 25, pp. 521-523, 2000.

[16]   M.Ibsen, M.K.Durkin, M.J.Cole, and R.I.Laming, "Optimised square passband fibre Bragg grating filter with in-band flat group delay response", Electron. Lett., vol. 34, pp.800-802, 1998.

[17]   G.P. Agrawal, "Nonlinear fiber optics", 2nd Edition, Academic Press Inc., 1995.

[18]   M.Ibsen, and R.I.Laming, "Fibre non-uniformity caused Bragg grating imperfections", Technical Digest OFC '99 San Diego 21-26 February 1999, paper FA1.

[19]   B.C. Thomsen, P. Petropoulos, H.L. Offerhaus, D.J. Richardson, and J.D. Harvey, "Characterization of a 10 GHz harmonically mode-locked erbium fiber ring laser using second harmonic generation frequency resolved optical gating", Technical Digest CLEO '99, Baltimore, 23-28 May 1999, paper CTuJ5.

[20]   M. Ibsen, M.K. Durkin, M.J. Cole, M.N. Zervas, and R.I. Laming, "Recent advances in long dispersion compensating fibre Bragg gratings", IEE Colloquium on Optical Fibre Gratings, paper 6, Aston University, UK ISSN 0963-3308, 1999.

[21]   A.D. Ellis, J.K. Lucek, D. Pitcher, D.G. Moodie, and D. Cotter, "Full 10x10Gbit/s OTDM data generation and demultiplexing using electroabsorption modulators", Electron. Lett., vol. 34, pp.1766-1767, 1998.

Figure captions

Fig.1 Calculated graphs of the electric field representation of the input 2.5ps soliton pulses (dashed lines) and the output 20ps square pulses (solid lines) in (a) the frequency and (b) the time domain.

Fig.2 (a) Refractive index modulation profile of the SSFBG performing shaping of solitons into square pulses; (b) spectral response and (c) time delay vs. wavelength of this FBG. In (b) the dashed line shows the calculated spectral response of the structure designed.

Fig.3 Numerical calculations showing the effect of non-ideal pulse inputs to the filtered output. The cases considered are: (a) soliton pulses of various widths (dotted line: 2.0ps, line-dot-dot: 2.3ps, line-dot-line: 2.3ps, dashed line: 3.0ps); (b) 2.5ps chirped soliton pulses (dashed line: $C = 0.1$, TBP = 0.342; line-dot-line: $C = 0.2$, TBP = 0.420; line-dot-dot: $C = 0.45$, TBP = 0.518); (c) Gaussian pulses of various widths (dashed line: 2.5ps, line-dot-line: 3.55ps); (d) 2.5ps soliton pulses of a mismatched central wavelength relative to the SSFBG (dashed line: mismatch of 0.4nm, line-dot-line: mismatch of 0.7nm, line-dot-dot: mismatch of 1.4nm). In all figures, the solid lines represent a 2.5ps soliton pulse input.

Fig.4 Two extreme cases of square pulses generated by SSFBG's with phase and amplitude imperfections in their structures (the noise parameters introduced are given in the text).

Fig.5 Experimental set-up for pulse shaping applications using SSFBG's.

Fig.6 (a) Measured power spectrum of the reflected pulses, and (b) the calculated power spectrum of the single square pulse shown in Fig.1. The inset shows the measured power spectrum of the input pulses (resolution of the measurements: 25pm).

Fig.7 Measured autocorrelation traces of (a) the 2.5ps soliton pulses, and (b) the reflected pulses; (c) shows the calculated autocorrelation function of the square pulses of Fig.1.

Fig.8 Optical sampling oscilloscope traces of (a) the input pulses and (b) the reflected off the SSFBG pulses

Fig.9 Measured optical sampling oscilloscope traces (a) and power spectra (b) for two cases of mismatch between the central wavelength of the laser source and the SSFBG; mismatches of 0.4nm (solid line) and 1.4nm (dashed line) are shown.

Fig.10 BER measurements of the 10Gbit/s square pulses.

Fig. 1

Fig. 2

Fig. 3

Fig.4

10GHz
soliton pulses
(monitor)

Shaped
output

EFRL

Circulator

EDFA

Strain-tunable
SSFBG
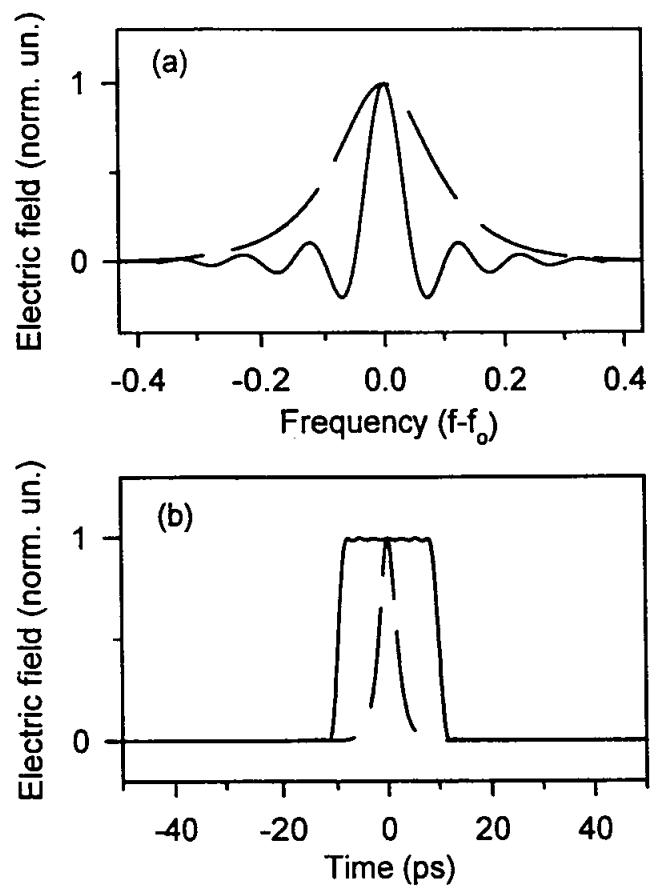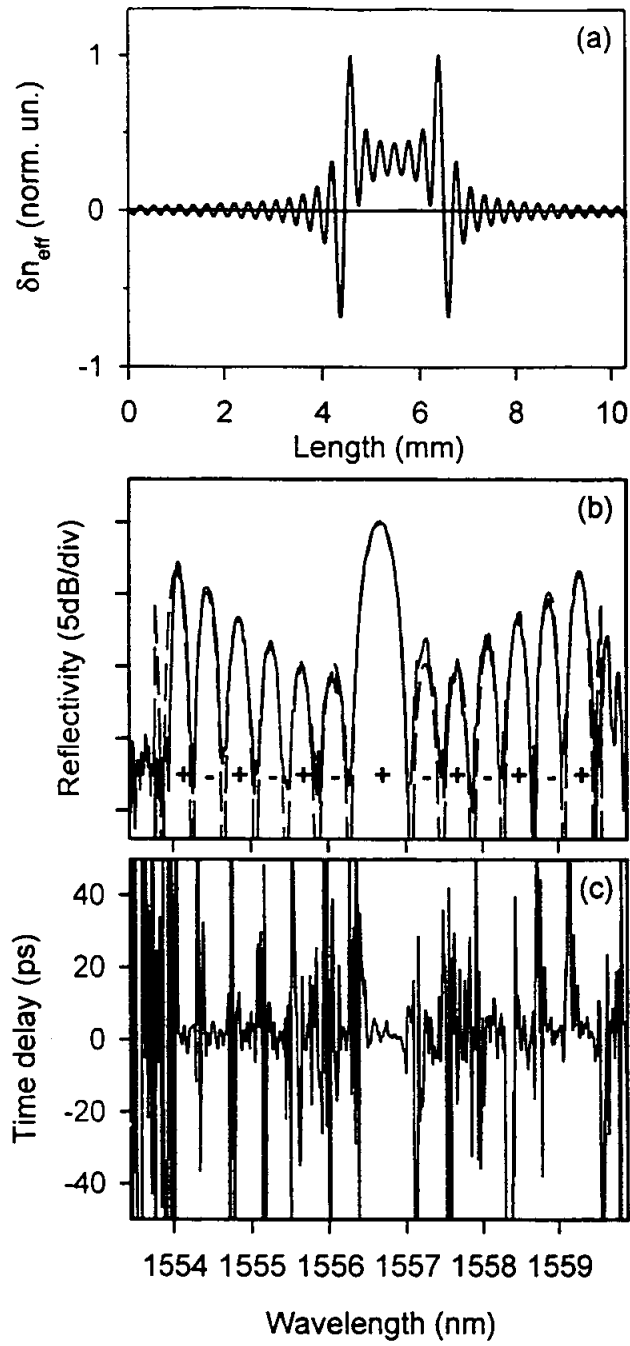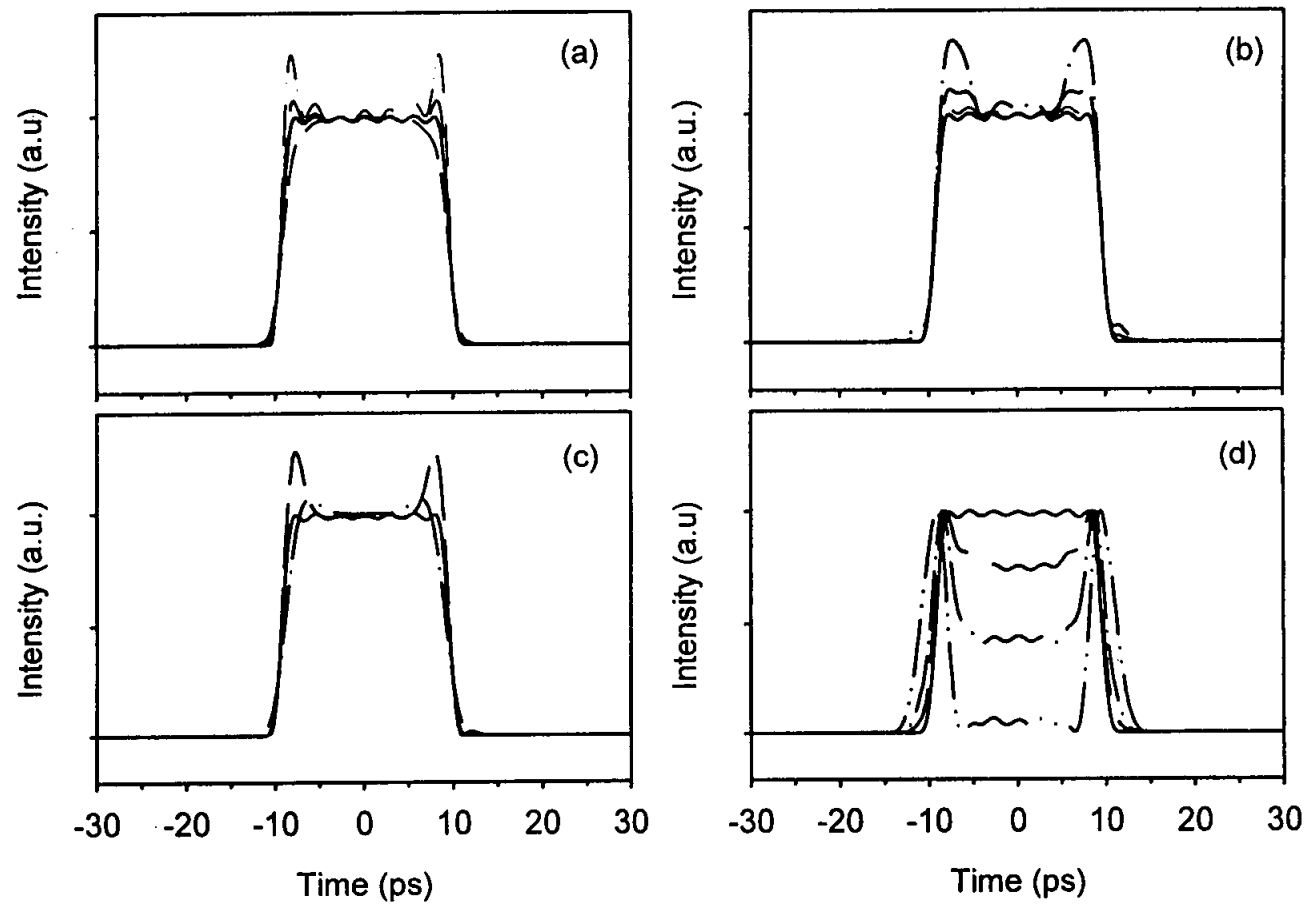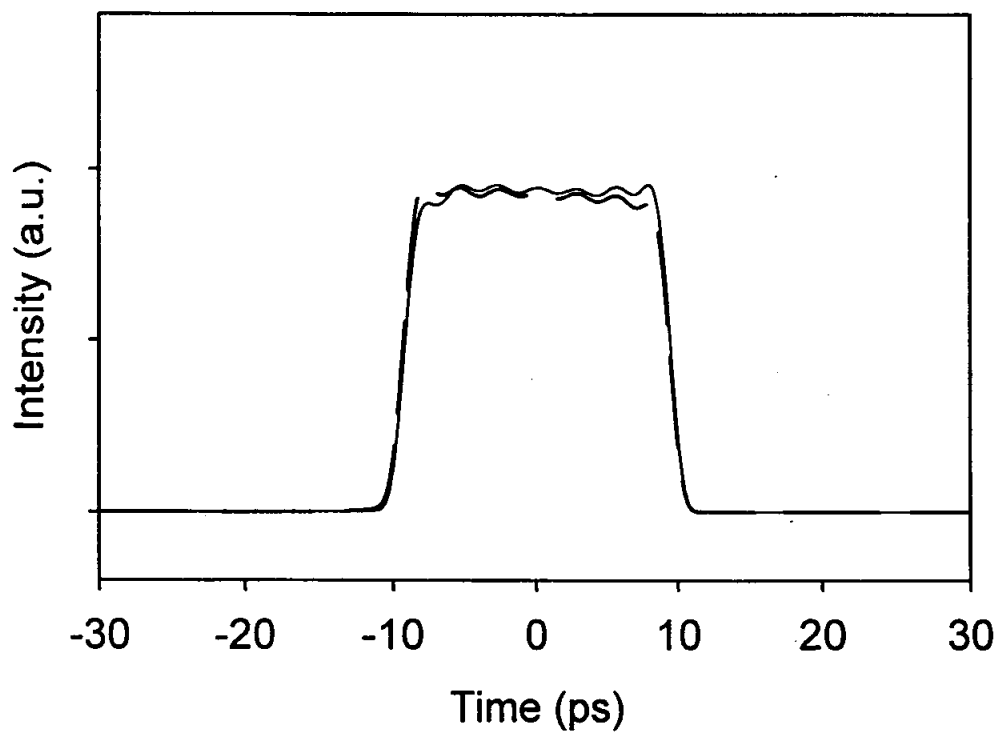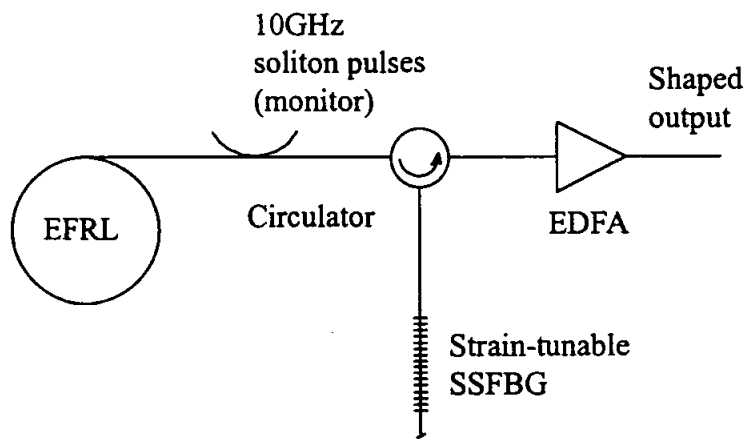
Fig. 5
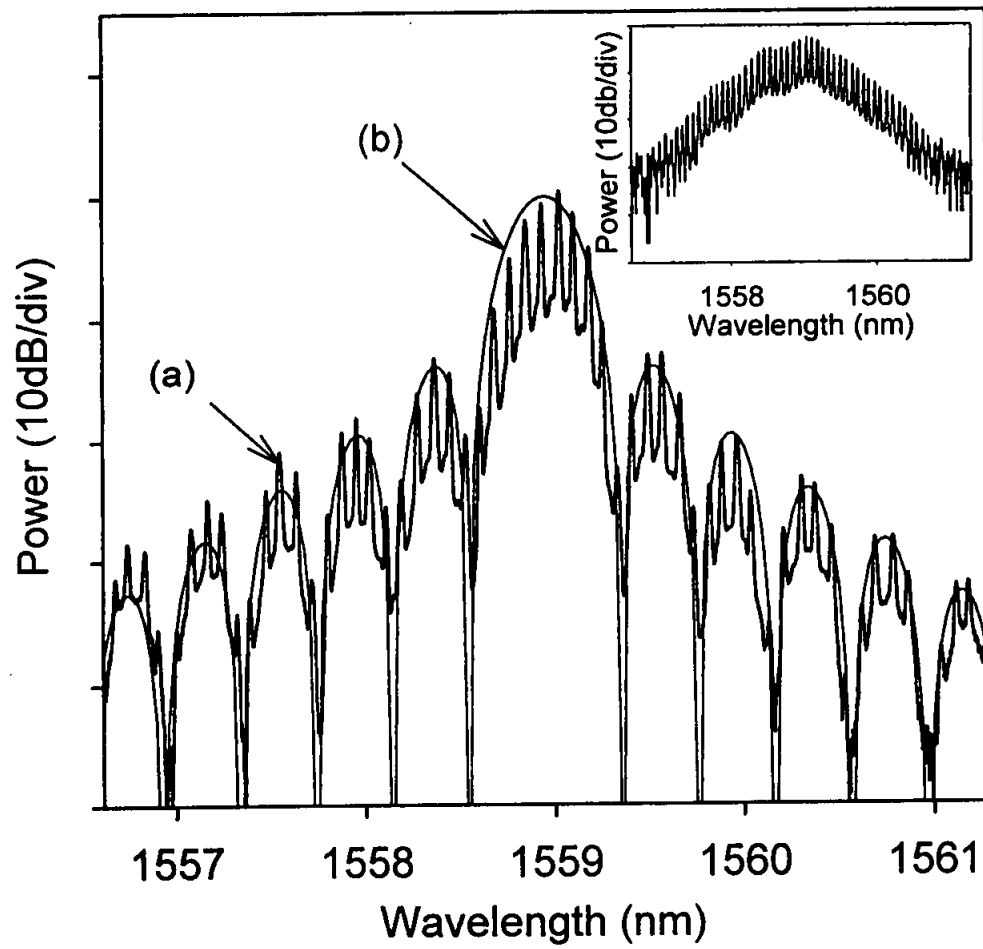
Fig.6

Fig.7

Fig.8

Fig. 9

Fig.10